Applied Surface Science 255 (2009) 4491–4496

Contents lists available at ScienceDirect

Applied Surface Science

journal homepage: www.elsevier.com/locate/apsusc

Electrical conductivity and optical properties of ZnO nanostructured thin film

Mujdat Caglar [a,*], Saliha Ilican [a], Yasemin Caglar [a], Fahrettin Yakuphanoglu [b]

[a] Anadolu University, Faculty of Science, Department of Physics, 26470 Eskisehir, Turkey
[b] Firat University, Faculty of Arts and Sciences, Department of Physics, 23169 Elazig, Turkey

ARTICLE INFO

Article history:
Received 29 July 2008
Received in revised form 2 October 2008
Accepted 21 November 2008
Available online 27 November 2008

Keywords:
ZnO
Nanostructured thin film
Sol–gel spin coating
Optical constants

ABSTRACT

The electrical conductivity, structural and optical properties of ZnO nanostructured semiconductor thin film prepared by sol–gel spin coating method have been investigated. The X-ray diffraction result indicates that the ZnO film has the polycrystalline nature with average grain size of 28 nm. The optical transmittance spectrum indicates the average transmittance higher than 90% in visible region. The optical band gap, Urbach energy and optical constants (refractive index, extinction coefficient, real and imaginary parts of the dielectric constant) of the film were determined. The electrical conductivity of the film dependence of temperature was measured to identify the dominant conductivity mechanism. The conductivity mechanism of the film is the thermally activated band conduction. The electrical conductivity and optical results revealed that the ZnO film is an n-type nanostructured semiconductor with a direct band gap of about 3.30 eV at room temperature.

1. Introduction

The unique and fascinating properties of nanostructured materials have triggered tremendous motivation among scientists to explore the possibilities of using them in technological applications. In particular, the electronic and optical properties of nanostructured materials have been of interest because of their potential applications in the fabrication of micro electronic and optoelectronic devices [1–6].

Zinc oxide, a member in the II–VI family with a wide band gap (3.3 eV) and a large excitonic binding energy (60 meV), possesses a unique position among materials owing to its superior and diverse properties such as piezoelectricity, chemical stability, biocompatibility, optical transparency in the visible region, high voltage–current nonlinearity, etc. Recently, significant progress in ZnO crystal quality has been made. Besides the nanostructures like nanotubes, nanorods, nanowalls, nanofibers, high-quality undoped and doped ZnO thin films have been grown with plasma-assisted molecular beam epitaxy [7], vapor transport deposition method [8], vacuum arc deposition [9] metalorganic chemical vapor deposition (MOCVD) [10], sol–gel process [11,12] and spray pyrolysis [13]. Such nanotubes, nanowires, nanoribbons and nanofibers have attracted extraordinary attention for their potential applications in applied fields such as field emission displays (FED), optical waveguides, solar cells, ultraviolet photodetectors, optical switches, and gas sensing [14–18].

There are several methods developed on synthesis of ZnO nanostructured thin films in literature. Alver et al. [19] obtained ZnO microrods by using spray pyrolysis and they studied the optical and structural properties of ZnO microrods, Li and Gao [20] reported ZnO nanocomposite films deposited onto glass substrates by magnetron sputtering in different atmospheres, Kale and Lu [21] reported ZnO microrods deposited by hydrothermal method and they studied structural, optical and morphological properties, Wu and Pan [22] reported ZnO nanofiber deposited by electrospinning technique. However, there are a few reports on the synthesis of them using a sol–gel method [23,24].

The sol–gel spin coating method has distinct advantages such as cost effectiveness, thin, transparent, multicomponent oxide layers of many compositions on various substrates, simplicity, excellent compositional control, homogeneity and lower crystallization temperature. There are no studies on the optical constants of spin coated ZnO nanostructured thin films in available literature. In this paper, we have investigated on the structural, optical and electrical properties of ZnO nanostructured thin film deposited by sol–gel spin coating method.

2. Experimental

The key to obtain good quality film using sol–gel spin coating method is the preparation of a clear, transparent and homogenous solution. In the present study, ZnO nanostructured thin film has been deposited by a sol–gel spin coating method onto

* Corresponding author. Tel.: +90 222 3350580/5738; fax: +90 222 3204910.
E-mail address: mcaglar@anadolu.edu.tr (M. Caglar).

0169-4332/$ – see front matter © 2008 Elsevier B.V. All rights reserved.
doi:10.1016/j.apsusc.2008.11.055

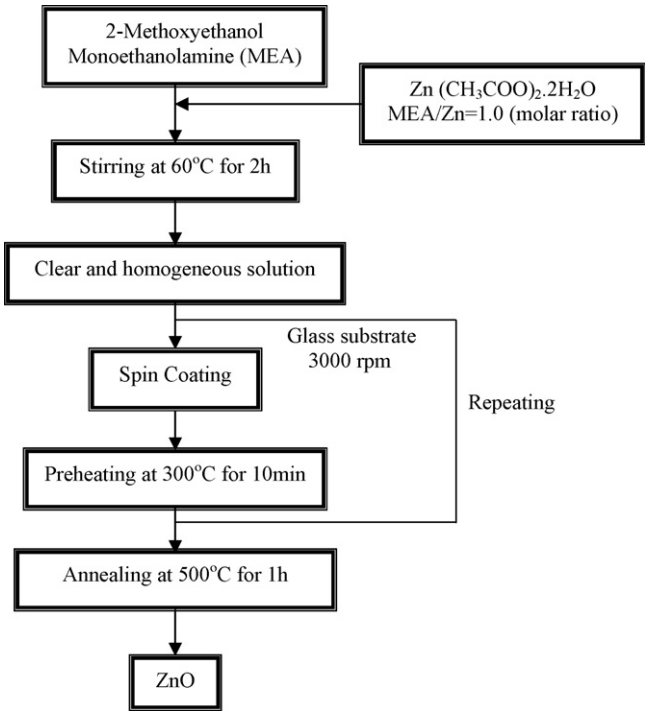

Fig. 1. The flow chart showing the procedure for preparing the ZnO nanostructured thin film.

glass substrate. Fig. 1 shows the flow chart of the preparation of ZnO nanostructured thin film. As a starting material, zinc acetate dihydrate [$Zn(CH_3COO)_2{\cdot}H_2O$] was used. 2-Methoxethanol and monoethanolamine (MEA) were used as a solvent and stabilizer, respectively. The molar ratio of MEA to zinc acetate dihydrate was maintained at 1.0 and the concentration of zinc acetate was 0.35 M. The solution was stirred at 60 °C for 2 h to yield a clear and homogeneous solution, which served as the coating solution after cooling to room temperature. The glass substrate was precleaned with a detergent, and then cleaned in methanol and acetone for 10 min using a Bandelin Sonorex RK100 ultrasonic cleaner and then cleaned with deionized water and dried. The coating solution was dropped into glass substrate, which was rotated at 3000 rpm for 30 s using a LAURELL WS-400B-6NPP/LITE spin coater. After the deposition, the film was dried at 300 °C for 10 min into a furnace to evaporate the solvent and remove organic residuals. The procedures from coating to drying were repeated nine times. The film was then inserted into a tube furnace and annealed in air at 500 °C for 1 h. The thickness of the film was determined with Mettler Toledo MX5 microbalance by using weighing method and found to be 357 nm. X-ray diffraction pattern was obtained with a RIGAKU RINT 2200 Series X-Ray Automatic Diffractometer using the CuKα radiations (λ = 1.54059 Å) in the range of 2θ between 20° and 60°. The diffractometer reflection was taken at room temperature. Surface morphology was studied using ZEISS EVO-50 model scanning electron microscope (SEM). Elemental analysis was performed using BRUKER AXS Energy Dispersive X-ray Spectroscopy (EDX), in which the electron energy used was 20 keV. The direct current conductivity (DC) measurements were performed with a KEITHLEY 6517A electrometer. The conductivity of ZnO nanostructured film was determined by the well-known hot probe method. The optical measurement of the film was carried out at room temperature using a SHIMADZU UV–VIS–NIR 3600 spectrophotometer in the wavelength range from 185 to 3300 nm.

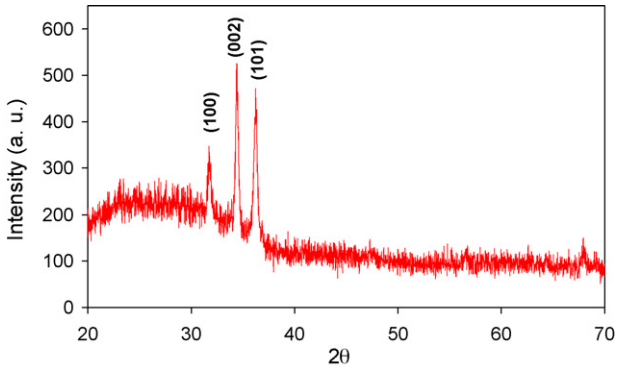

Fig. 2. X-ray diffraction pattern of the ZnO nanostructured thin film.

3. Results and discussion

3.1. Structural and morphological properties of the ZnO nanostructured thin film

The crystal structure and orientation of ZnO nanostructured thin film have been investigated by X-ray diffraction (XRD) method. The XRD pattern of the film is shown in Fig. 2. The XRD result suggests that the ZnO thin film has the polycrystalline structure. The film was crystallized with the hexagonal wurtzite structure and a preferred orientation of (0 0 2). The diffraction peaks corresponding to (1 0 1) and (1 0 0) planes of ZnO hexagonal phase were observed. The lattice spacing (d), percentage error in d value, angle of diffraction (2θ) at the phases identified along with (h k l) planes of the ZnO nanostructured film are given in Table 1.

The lattice constants for hexagonal ZnO film are reported in Joint Committee on Powder Diffraction Standards (JCPDS) standard data a = 3.24982 Å and c = 5.20661 Å [25]. Lattice constants are obtained by the following equation,

$$\frac{1}{d^2_{(hkl)}} = \frac{4}{3}\left(\frac{h^2+hk+k^2}{a^2}\right) + \frac{l^2}{c^2} \quad (1)$$

The lattice constants calculated by using Eq. (1) are a = 3.25452 Å and c = 5.20980 Å. The calculated lattice constants are in good agreement with 36-1451 JCPDS standard data [25]. These values show that the ZnO film grows preferentially with the (0 0 2) axis perpendicular to the substrate surface. The grain size (D) of the film was calculated for preferential orientations to have information about their crystallinity levels. The Scherrer equation was used to calculate the average crystallite size of ZnO nanostructured film using its (0 0 2) reflection [26]. The average grain size of the ZnO film was found to be 28 nm.

The texture coefficient (TC) represents the texture of particular plane, deviation of which from unity implies the preferred growth. Quantitative information concerning the preferential crystallite orientation was obtained from the different texture coefficient $TC(hkl)$ defined as [27]

$$TC(hkl) = \frac{I(hkl)/I_o(hkl)}{N^{-1}\sum_n I(hkl)/I_o(hkl)} \quad (2)$$

where $I(hkl)$ is the measured relative intensity of a plane (hkl), $I_o(hkl)$ is the standard intensity of the plane (hkl) taken from the JCPDS data, N is the reflection number and n is the number of diffraction peaks. A sample with randomly oriented crystallite presents $TC(hkl)$ = 1, while the larger value, the larger abundance of crystallites oriented at the (hkl) direction. The texture coefficient was calculated for the highly oriented peak of (0 0 2) and is given in Table 1.

Table 1
2θ, d, $d\%$, I/I_o, TC values for the ZnO nanostructured thin film.

(h k l)	2θ	d (Å)	$d\%$	I/I_o	TC
(1 0 0)	31.721	2.8185	0.15	36.1	0.769
(0 0 2)	34.400	2.6049	0.06	100.0	2.131
(1 0 1)	36.239	2.4768	0.04	86.6	1.846

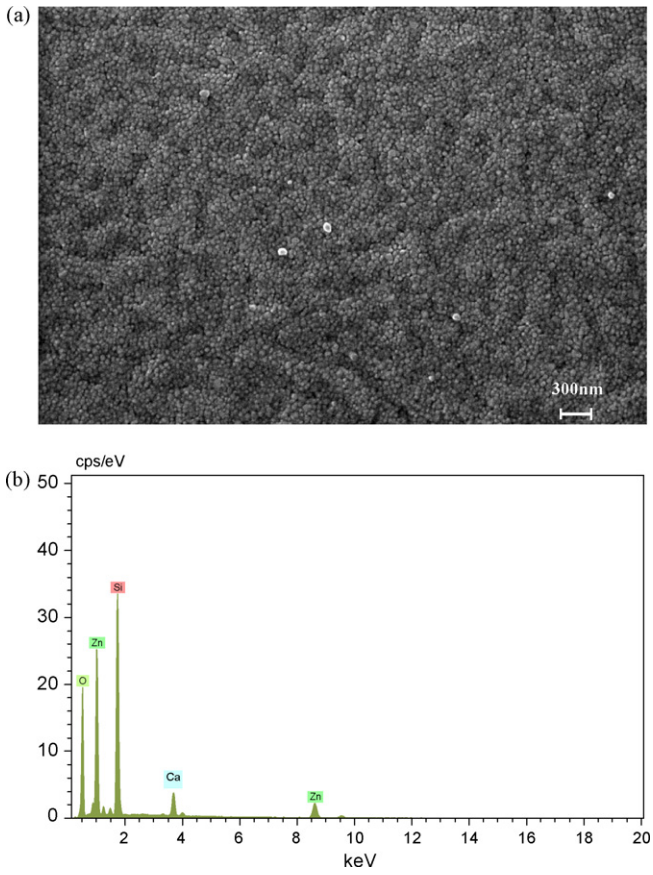

Fig. 3. SEM image (a) and EDX analysis (b) of the ZnO nanostructured thin film.

Fig. 3a shows SEM micrograph of ZnO nanostructured thin film. The film exhibits a porous nanostructure and the spherical crystalline particle size is approximately 40 nm. In the literature, ZnO nanostructures having 9–250 nm have been reported [28,29].

To check the chemical composition of the film, an energy-dispersive X-ray (EDX) spectroscopy analysis was performed. Fig. 3b shows the EDX spectrum of ZnO nanostructured thin film. Five peaks have been clearly observed from the spectrum, which are identified as zinc, oxygen, silicon and calcium. The presence of the calcium and silicon peak in the spectrum is due to the glass substrate. It was observed that the film is only composed of zinc and oxygen.

3.2. Optical band gap and Urbach energies of the ZnO nanostructured thin film

In order to analyze the optical properties of the ZnO nanostructured thin film, the optical transmittance and reflectance spectrum were obtained. The transmittance and reflectance spectra of the film are shown in Fig. 4. The average value of optical transmission for the ZnO thin film in the visible range (400–800 nm) was found to be 93%. This suggests that the film has a high transparency. The optical band gap can be calculated by the

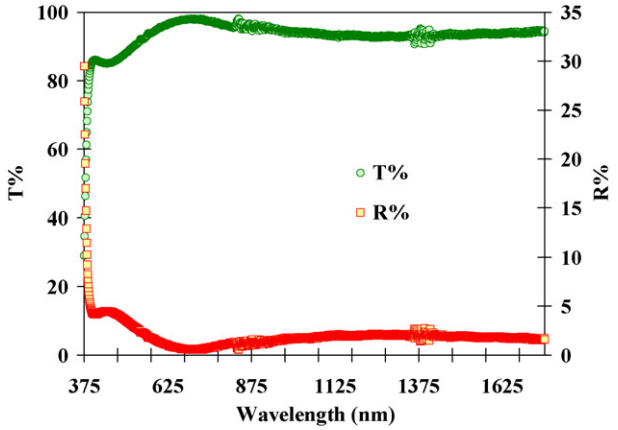

Fig. 4. Optical transmittance and reflectance spectra of the ZnO nanostructured thin film.

following relation [30],

$$(\alpha h\nu) = A(h\nu - E_g)^{1/2} \tag{3}$$

where α is the absorption coefficient, $h\nu$ the photon energy, A a constant, and E_g is the optical band gap. It is evaluated that the optical band gap of the ZnO nanostructured film has a direct optical transition [31,32]. It is well known that direct transitions across the band gap are feasible between the valence and the conduction band edges in k-space. In this transition process, the total energy and momentum of the electron-photon system must be conserved. Fig. 5a shows plot of $(\alpha h\nu)^2$ vs. photon energy. The value of the direct band gap E_g was found to be 3.30 eV. The optical band gap of ZnO nanostructured thin film is lower than that of amorphous zinc oxide thin films [33]. The optical band gap dependence of grain size is expressed as [34],

$$E_g(\text{nanocrystal}) = E_g(\text{bulk}) + \frac{\pi^2\hbar^2}{2R^2}\left(\frac{1}{m_e^*} + \frac{1}{m_h^*}\right) \tag{4}$$

where m_e^* and m_h^* are the effective masses of the electrons and holes, respectively, R the radius of the particle, E_g (nanocrystal) is the band gap of nanocrystal ZnO and E_g (bulk) is the optical band gap of bulk ZnO. The optical band gap of bulk ZnO is 3.3 eV [35]. The effective masses of electrons and holes of ZnO are $0.24m_o$ and $0.45m_o$, respectively [36]. The E_g (nanocrystal) for the ZnO was found to be 3.312 eV and the calculated enhancement in band gap for 28 nm particle size was found to be about 12.1 meV. The obtained band gap for the ZnO nanostructured thin film is lower than that of optical band gap of ZnO thin film with 8 nm grain size (3.381 eV) [37]. This suggests that the optical band gap of the ZnO film decreased with increasing grains size. Furthermore, in literature, it has been reported that ZnO nanoparticles change the optical band gap and optical band gap increases with decreasing size of the nanoparticles [38–41].

The absorption coefficient near the fundamental absorption edge is exponentially dependent on the incident photon energy and obeys the empirical Urbach relation. The Urbach energy can be calculated by the following relation [42],

$$\alpha = \alpha_o \exp\left[\frac{h\nu - E_I}{E_U}\right] \tag{5}$$

where E_I and α_o are constants and E_U is the Urbach energy which refers to the width of the exponential absorption edge. Fig. 5b shows the variation of ln α vs. photon energy for the film. The value of the Urbach energy E_U was found to be 67 meV. The dependence of the optical absorption coefficient with photon energy may arise from trapping levels at grain boundaries. The density of these

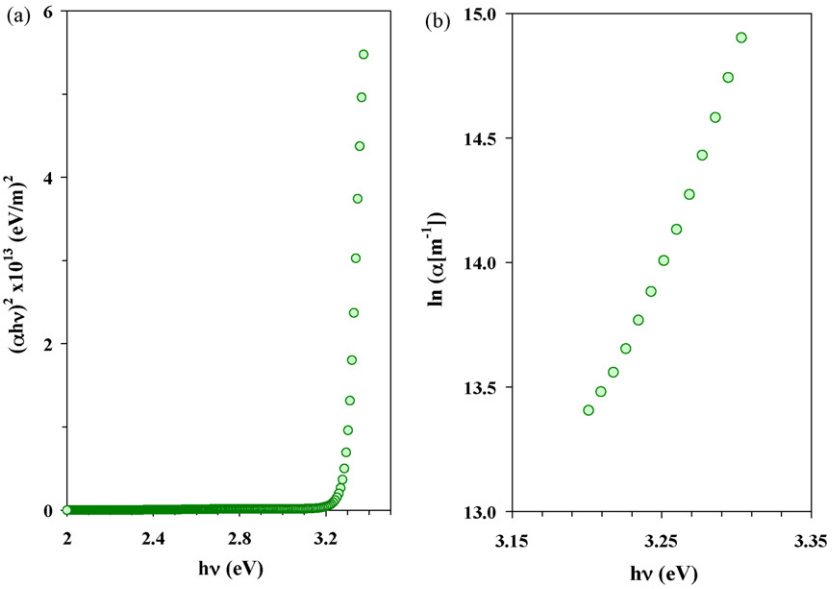

Fig. 5. Plots of $(\alpha h\nu)^2$ vs. energy and Urbach energy of the ZnO nanostructured thin film.

states falls off exponentially with energy, which is consistent with the theory of Tauc [43]. Eq. (6) can be rewritten as

$$\alpha = \alpha_o \exp\left[\frac{\beta}{kT}(E - E_I)\right] \quad (6)$$

where β is called steepness parameter, which characterizes the broadening of the absorption edge due to the electron-phonon interaction or exciton–phonon interaction. If the width of the edge, E_U, is related to the slope of Eq. (6), the β parameter is found as $\beta = kT/E_U$. The β value was calculated using this relationship and taking $T = 300$ K and are found to be 38.63×10^{-2}.

3.3. Electrical conductivity properties of the ZnO nanostructured thin film

The plot of σ vs. $1000/T$ of ZnO nanostructured thin film is shown in Fig. 6. The conductivity curve of the film indicates different three regions (I, II and III). The regions I and III correspond to different conduction mechanisms. In I and III regions, the electrical conductivity increases with increasing temperature, as the temperature is increased and in turn, more charge carriers overcome the activation energy barrier and participate in the electrical conductivity.

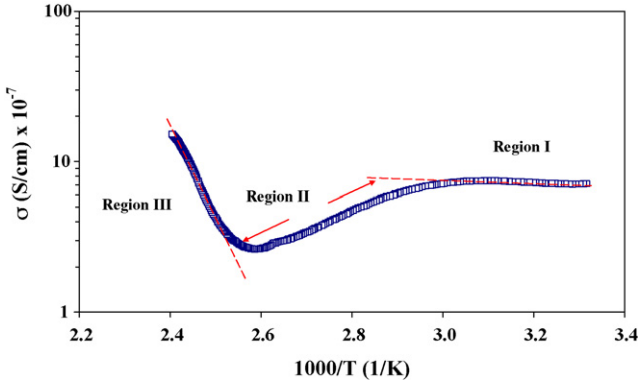

Fig. 6. Plot of σ vs. $1000/T$ of the ZnO nanostructured thin film.

The electrical conductivity of the ZnO film can be analyzed by the well-known relation,

$$\sigma = \sigma_o \exp\left(-\frac{E}{kT}\right) \quad (7)$$

where σ_o is the pre-exponential factor and E is the activation energy for electrical conductivity. E_I and E_{III} activation energy values for I and III regions were calculated from the linear portions of Fig. 6, respectively. The obtained E_I and E_{III} values were found to be 25.8 meV and 1.32 eV, respectively. The magnitude of the activation energy $E_{III} = 1.32$ eV obtained from conductivity data is small comparison with optical band gap energy ($E_g = 3.30$ eV). This confirms that while the activation energy corresponds to the energy required for conduction from one site to another, the optical band gap corresponds to another transition. These activation energies at different temperature regions (I and III) indicate the presence of two donor levels. These levels are the shallow and deep donor levels in the band gap of the ZnO semiconductor. The value of 25.8 meV corresponds to the shallow donor level, while the value of 1.32 eV corresponds to the deep donor level. Thus, it is evaluated that in region III, the electrical conductivity of the ZnO thin film is thermally activated from the deep donor level to the conduction band. The region II is a transition region, in which more charge carriers are ionized from the shallow donor level and then, the charge carriers are depleted and in turn, the electrical conductivity decreases with increase of temperature up to activation of charge charges in deep donor level start. Room temperature electrical conductivity value was found to be 7.261×10^{-7} S/cm. This conductivity value is higher than that of nanophase zinc oxide prepared by arrested precipitation method [44]. Furthermore, Lee et al. [45] reported that the conductivity for nanophase ZnO having particle size of 60 nm is in the range 2×10^{-6} to 2×10^{-4} S/cm at 450–600 °C. The increase in conductivity of ZnO nanostructured thin film studied can be explained as the conductivity of the ZnO film is attributed to the trapping of electrons in the grain boundaries. The grain size (28 nm) of ZnO nanostructured studied is less than the Debye length (~30 nm for nano ZnO) and this suggests accumulation of electrons at grain boundary and in turn, electrical conductivity increases. The film is an n-type semiconductor material due to the

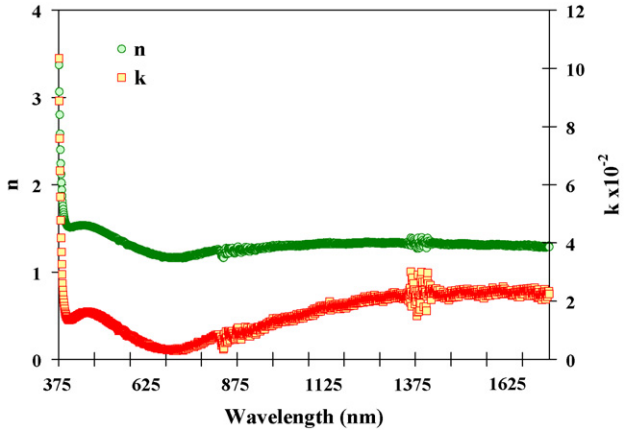

Fig. 7. The variation of refractive index and extinction coefficient of the ZnO nanostructured thin film.

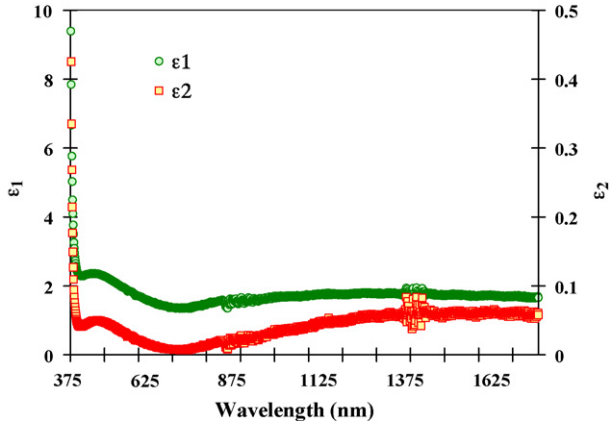

Fig. 8. The variation of real (ε_1) and imaginary (ε_2) parts of the dielectric constant of the ZnO nanostructured thin film.

presence of intrinsic defects such as oxygen vacancies and Zn interstitials [46].

3.4. The refractive index and dielectric constants of the ZnO nanostructured thin film

The complex refractive index and dielectric function characterize the optical properties of any solid material. The dispersion plays an important role in the research for optical materials; because, it is a significant factor in optical communication and in designing devices for spectral dispersion. The optical properties of the film have been investigated by spectrophotometric measurement of transmittance, T, and reflectance, R, at normal incidence in the wavelength range of 375–1750 nm. The refractive index of the film was calculated by the following relation [47],

$$R = \frac{(n-1)^2 + k^2}{(n+1)^2 + k^2} \tag{8}$$

where k ($k = \alpha\lambda/4\pi$) is the extinction coefficient. As shown in Fig. 7, the refractive index dependence of wavelength was plotted. The refractive index of the film decreases with the increasing of wavelength in the visible region, while it increases in the ultraviolet region, i.e. anomalous dispersion. The extinction coefficient k dependence of wavelength is shown in Fig. 7. The k values of the film decrease up to certain value of wavelength and then, increase. The fundamental electron excitation spectrum of the film is described by means of a frequency dependence of the complex electronic dielectric constant. The dielectric constant is defined as, $\varepsilon(\omega) = \varepsilon_1(\omega) + i\varepsilon_2(\omega)$ and real and imaginary parts of the dielectric constant are related to the n and k values. The ε_1 and ε_2 values were calculated using the formulas [48],

$$\varepsilon_1 = n^2 - k^2 \tag{9}$$

$$\varepsilon_2 = 2nk \tag{10}$$

Fig. 8 shows ε_1 and ε_2 values dependence of photon energy. ε_1 and ε_2 values of the film increase with increasing energy. The real and imaginary parts of the dielectric constant indicate the same pattern and the values of real part are higher than imaginary part. It can be seen that the real and imaginary parts of the dielectric constant decrease with increasing wavelength in the visible region while they increase in the ultraviolet region.

4. Conclusions

The optical, structural and electrical properties of ZnO nanostructured thin film have been investigated. The X-ray diffraction spectrum indicates that the film has the polycrystalline structure. In regions I and III, the electrical conductivity of ZnO nanostructured is controlled by the thermally activated mechanism. The optical band gap and optical constants (refractive index, extinction coefficient, real and imaginary parts of the dielectric constant) of ZnO nanostructured thin film were determined.

Acknowledgement

This work was supported by Anadolu University Commission of Scientific Research Projects under Grant no. 061039.

References

[1] M. Krunks, A. Katerski, T. Dedova, I. Oja Acik, A. Mere, Solar Energy Mater. Solar Cell. 92 (2008) 1016.
[2] W.P. Tai, K. Inoue, Mater. Lett. 57 (2003) 1508.
[3] C. Monat, B. Alloing, C. Zinoni, L.H. Li, A. Fiore, Nano Lett. 6 (2006) 1464.
[4] T. Piok, S. Gamerith, C. Gadermaier, H. Plank, F.P. Wenzl, S. Patil, R. Montenegro, T. Kietzke, D. Neher, U. Scherf, K. Landfester, E.J.W. List, Adv. Mater. 15 (2003) 800.
[5] B.L. Allen, P.D. Kichambare, A. Star, Adv. Mater. 19 (2007) 1439.
[6] A.L. Briseno, S.C.B. Mannsfeld, X. Lu, Y. Xiong, S.A. Jenekhe, Z. Bao, Y. Xia, Nano Lett. 7 (2007) 668.
[7] Y. Jian-Feng, L. You-Ming, L. Hong-Wei, L. Yi-Chun, L. Bing-Hui, F. Xi-Wu, Z. Jun-Ming, J. Cryst. Growth 280 (2005) 206.
[8] M.K. Li, D.Z. Wang, S. Ding, Y.W. Ding, J. Liu, Z.B. Liu, Appl. Surf. Sci. 253 (2007) 4161.
[9] N. Parkansky, G. Shalev, B. Alterkop, S. Goldsmith, R.L. Boxman, Z. Barkay, L. Glikman, H. Wulff, M. Quaas, Surf. Coat. Tech. 201 (2006) 2844.
[10] S.W. Kim, S. Fujita, M.S. Yi, D.H. Yoon, Appl. Phys. Lett. 88 (2006) 253114.
[11] S. Ilican, Y. Caglar, M. Caglar, F. Yakuphanoglu, J. Cui, Phys. E: Low-dimen. Syst. Nanostruct. 41 (2008) 96.
[12] S. Ilican, Y. Caglar, M. Caglar, F. Yakuphanoglu, Appl. Surf. Sci. 255 (2008) 2353.
[13] S. Ilican, Y. Caglar, M. Caglar, F. Yakuphanoglu, Phys. E: Low-dimen. Syst. Nanostruct. 35 (2006) 131.
[14] L. Dong, J. Jiao, D.W. Tuggle, J.M. Petty, S.A. Ellif, M. Coulter, Appl. Phys. Lett. 82 (2003) 1096.
[15] M. Law, D.J. Sirbuly, J.C. Johnson, J. Goldberger, R.J. Saykally, P. Yang, Science 305 (2004) 1269.
[16] M. Law, L.E. Greene, J.C. Johnson, R. Saykally, P. Yang, Nat. Mater. 4 (2005) 455.
[17] H. Kind, H. Yan, B. Messer, M. Law, P. Yang, Adv. Mater. 14 (2002) 158.
[18] J.W.P. Hsu, D.R. Tallant, R.L. Simpson, N.A. Missert, R.G. Copeland, Appl. Phys. Lett. 88 (2006) 252103.
[19] U. Alver, T. Kılınç, E. Bacaksız, T. Küçükömeroğlu, S. Nezir, I.H. Mutlu, F. Aslan, Thin Solid Films 515 (2007) 3448.
[20] Z.W. Li, W. Gao, Thin Solid Films 515 (2007) 3323.
[21] R.B. Kale, S.Y. Lu, J. Phys-Condens. Mater. 19 (2007) 096209.
[22] H. Wu, W. Pan, J. Am. Ceram. Soc. 89 (2006) 699.
[23] Y. Zhang, B. Lin, Z. Fu, C. Liu, W. Han, Opt. Mater. 28 (2006) 1192.
[24] J. Li, S. Srinivasan, G.N. He, J.Y. Kang, S.T. Wu, F.A. Ponce, J. Cryst. Growth 310 (2008) 599.

[25] Powder Diffraction File 36-1451 for hexagonal Zinc Oxide (1997 JCPDS-International center for Diffraction data).
[26] B.D. Cullity, S.R. Stock, Elements of X-Ray Diffraction, 3rd ed., Prentice Hall, Upper Saddle River, NJ, 2001.
[27] C.S. Barret, T.B. Massalski, Structure of Metals, Pergamon Press, Oxford, 1980.
[28] Y.S. Kim, W.P. Tai, S.J. Shu, Thin Solid Films 491 (2005) 153.
[29] S. Mridha, D. Basak, Mater. Res. Bull. 42 (2007) 875.
[30] J.I. Pankove, Optical Processes in Semiconductors, Prentice-Hall Inc., Englewoord Cliffs, NJ, 1971.
[31] M. Guo, C.Y. Yang, M. Zhang, Y. Zhang, T. Ma, XiDong Wang, XinDong Wang, Electrochim. Acta 53 (2008) 4633.
[32] U.N. Maiti, P.K. Ghosh, S. Nandy, K.K. Chattopadhyay, Physica B 387 (2007) 103.
[33] J.M. Khoshman, M.E. Kordesch, Thin Solid Films 515 (2007) 7393.
[34] Y. Kayanuma, Phys. Rev. B 38 (1988) 9797.
[35] R.P. Casero, A.G. Llorente, O.P.Y. Moll, W. Seiler, R.M. Defourneau, D. Defourneau, E. Millon, J. Perrie're, P. Goldner, B. Viana, J. Appl. Phys. 97 (2005) 054905.
[36] E.M. Wong, P.C. Searson, Appl. Phys. Lett. 74 (1999) 2939.
[37] M. Berber, V. Bulto, R. Kliß, H. Hahn, Scripta Mater. 53 (2005) 547.
[38] H. Yano, J. Sugiyama, A.N. Nakagaito, M. Nogi, T. Matsuura, M. Hikita, K. Handa, Adv. Mater. 17 (2005) 153.
[39] R.J. Nussbaumer, W.R. Caseri, P. Smith, T. Tervoort, Macromol. Mater. Eng. 288 (2003) 44.
[40] V. Srikant, D.R. Clarke, J. Appl. Phys. 83 (1998) 5447.
[41] M.G. Kakazey, V.A. Melnikova, T. Sreckovic, T.V. Tomila, M.M. Ristic, J. Mater. Sci. 34 (1999) 1691.
[42] F. Urbach, Phys. Rev. 92 (1953) 1324.
[43] J. Tauc, Amorphous and Liquid Semiconductors, Plenum Press, New York, 1974 .
[44] J. Jose, M. Abdul Khadar, Mater. Sci. Eng. A-Struct. 304–306 (2001) 810.
[45] J. Lee, J.H. Hwang, J.J. Mashek, T.O. Mason, A.E. Miller, R.W. Siegel, J. Mater. Res. 10 (1995) 2295.
[46] Ç. Kılıç, A. Zunger, Phys. Rev. Lett. 88 (2002) 095501.
[47] F. Abeles (Ed.), Optical Properties of Solids, North-Holland, Publishing Company, London, UK, 1972.
[48] J.N. Hodgson, Optical Absorption and Dispersion in Solids, Chapman and Hall Ltd., 11 New fetter Lane London EC4, 1970.